energies

MDPI

Article

An Online Archimedes Optimization Algorithm Identifier-Controlled Adaptive Modified Virtual Inertia Control for Microgrids

Asmaa Fawzy [1], Youssef Mobarak [1,2], Dina S. Osheba [3], Mahmoud G. Hemeida [4,*], Tomonobu Senjyu [5] and Mohamed Roshdy [1]

[1] Department of Electrical Engineering, Faculty of Energy Engineering, Aswan University, Aswan 81528, Egypt
[2] Faculty of Engineering, King Abdulaziz University, Rabigh 21911, Saudi Arabia
[3] Department of Electrical Engineering, Faculty of Engineering, Menoufia University, Shebin El Kom 32511, Egypt
[4] Minia Higher Institute of Engineering, Minya 61111, Egypt
[5] Department of Electrical and Electronics Engineering, Faculty of Engineering, University of the Ryukyus, Nishihara 903-0213, Japan
* Correspondence: mahmoud_hmeda2000@aswu.edu.eg; Tel.: +20-106-602-8909

Abstract: Single widespread employment of renewable energy sources (RESs) contributes to the shortage in the inertia of the microgrid (MG). After this, frequency stability may regress as a result of power imbalance or minor load fluctuations. This paper proposes an explicit adaptive modified virtual inertia control (VIC) based on an online Archimedes optimization algorithm (AOA) identifier for MG containing thermal, wind, and solar photovoltaic power plants. The Rung Kutta approach is used to construct the proposed online identifier, which acts as a model of the MG. AOA predicts the coefficients of the online identifier based on the input and output of MG to mimic the frequency deviation of the MG online. AOA estimates online the inertia and damping coefficients of the VIC system with an energy storage device based on online AOA identifier coefficients. The frequency deviation of the MG based on the proposed explicit adaptive modified VIC is compared with the conventional VIC based on fixed parameters and the VIC system based on optimal parameters using AOA offline under mutation in loads, weather-dependent input, and MG parameters using MATLAB/Simulink software. Furthermore, the proposed explicit adaptive modified VIC based on an online AOA identifier is evaluated with the adaptive VIC system based on fuzzy logic control, which adjusts only the inertial gain online. The simulation results demonstrate the capabilities of the proposed explicit adaptive modified VIC to improve the frequency stability and enhance low-inertia islanded MGs with RESs.

Keywords: explicit self-tuning adaptive control (ESTC); system identification; islanded microgrid (MG); Archimedes optimization algorithm (AOA); renewable energy sources (RESs); adaptive modified virtual inertia control (VIC)

Citation: Fawzy, A.; Mobarak, Y.; Osheba, D.S.; Hemeida, M.G.; Senjyu, T.; Roshdy, M. An Online Archimedes Optimization Algorithm Identifier-Controlled Adaptive Modified Virtual Inertia Control for Microgrids. *Energies* **2022**, *15*, 8884. https://doi.org/10.3390/en15238884

Academic Editor: Silvio Simani

Received: 12 October 2022
Accepted: 22 November 2022
Published: 24 November 2022

1. Introduction

In recent decades, RESs such as solar, wind energy, and micro-turbines have been growing dramatically due to the focus on the protection of the environment from hazardous pollutants, the reduction of fuel consumption, and the stimulation of economic growth [1].

RES has replaced many traditional grid units to improve system dependability and decrease voltage droop and transmission system losses. Otherwise, its impact on the power systems performance is a deficiency of system inertia [2] and alters the system's parameters, which in turn impacts the active power perturbations. In order to deal with the change in the power system parameters, several studies have recently turned to system identification [3,4]. Simulation and modeling software are required to analyze the MG

system [5]. Recently, system identification has gained prominence as a useful technique for defining the external behavior of the system [6]. An adaptive neuro-fuzzy inference system and a radial bias function neural network (RBFNN) have been used as a modeling approach for forecasting the power response of a wind turbine [7] and the nonlinear behavior of the photovoltaic (PV) power plant [8].

Indirect adaptive controllers are thought to be more powerful than intelligent controllers for reducing oscillations and enhancing power system stability as they combine an online identifier and a controller. For online model identification and online monitoring of changes to system parameters, the parameter's identifier is used. After that, the controller is updated. The regulation of motor drive speed has been suggested, using an indirect adaptive controller [9–11]. An explicit adaptive power system stabilizer inhibits perturbations and improves system reliability [12,13]. This technique is suitable for online applications as it offers unique modeling, training, and stability characteristics. Therefore, this study uses the proposed explicit adaptive modified VIC based on an online AOA identifier, where the online identifier changes the gains of the proposed VIC (i.e., inertia and damping coefficients) to handle loads/renewables uncertainties. As a result, the power variation of the energy storage system is used for inertia support to the MG studied.

Depending on how connected the MG is to the grid, the grid works in either the grid-connected mode or the islanded mode. Due to load changes and renewable generation sources, regulation of MG in the islanded mode is difficult [14,15]. Therefore, this study tries to maintain the frequency stability of the islanded MGs.

The frequency oscillations of the system will be substantial as RESs can penetrate MGs at a greater rate. As a result, frequency regulation is made more difficult when there is a discrepancy between power generation and load demand. The system's inertia and stability are increased by the strong resemblance of MGs to real synchronous generators. The response of primary movers is simulated using a virtual synchronous generator (VSG). The VIC improves the stability of the islanded MG using an energy storage system (ESS), such as a battery ESS (BESS), flywheel ESS, or superconducting magnetic energy storage (SMES) [1,16,17]. The majority of early investigations used the VIC concept, which focuses on the derivative technique to boost the performance of the power systems as multiple high voltage direct current (HVDC) interconnected power systems [18–20]. The frequency dynamic performance of an islanded MG under contingencies has been improved using the H-infinite robust control method by the VIC [21], and VIC-based CDM used the chaotic crow search algorithm (CCSA) [22]. The VSG uses virtual primary and secondary controllers in addition to the virtual rotor concept [23]. When the distributed generation sources and the time delay between them increase, affecting frequency stability, the robust model predictive controller (RMPC)-based VIC [24] and a self-adaptive VIC incorporating fuzzy logic [25] are adopted. A robust VIC for a low-inertia microgrid has been proposed to minimize the undesirable effects of a phase-locked loop (PLL), and improve the microgrid frequency stability [26]. A VIC based on robust model predictive controller (RMPC) which takes into consideration the time delays in microgrids improves frequency stability [24]. The frequency regulation issue of an MG has been improved using a modified golden jackal optimization (mGJO) based on an adaptive fuzzy PID structure with a derivative filter (AFPIDF) controller with VIC [27]. To regulate the system frequency, a VIC is applied to the superconducting magnetic energy storage (SMES) [28], a VI scheme predicated on electric vehicles (EVs) [29], and a VIC and PID based on an intelligent Salp swarm algorithm (SSA) [30].

Recent studies have considered both the VI and virtual damping to guarantee reliability and consistency in the frequency control investigation. In addition, the frequency response improves with higher levels of inertia and damping; in real-world applications, however, raising these values too high would result in overshoots and higher building costs. The frequency stability of low-inertia power systems has been enhanced using the modified VIC [31] for the Egyptian power system (EPS) [32], the MPC-controlled VSG [33], the synthetic inertia control (SIC) system based on electric vehicles (EVs) [34], the novel

analytical tuning approach under the influence of VIC [35], and the adaptive VIC based on MPC [36]. Novel modeling for VIC and a cascade controller based on a combination of the FOCs and 3DOF as a secondary controller have been presented to improve the MG frequency performance [37].

In this study, an online AOA identifier controlled explicit adaptive modified VIC for an islanded MG was designed which takes into consideration the high penetration of RESs, which simulates damping and inertia features simultaneously to improve system performance and stability under many different system operations. The virtual damping component depends on the system's frequency deviation in terms of the fast system's setting time when the virtual inertia component is produced using a derivative technique. In contrast, most literature suggests that the design of VIC systems relies on constant inertia and damping coefficient values, which may have a substantial impact on the frequency stability of microgrids at various levels of renewable energy penetration, where fixed values of virtual inertia and damping coefficients or inappropriate value selections may lead to higher frequency oscillations. To overcome such a problem, an explicit adaptive modified VIC is proposed. In this concept, the virtual inertia and damping coefficients are automatically adjusted using Archimedes optimization algorithm (AOA) based on an online AOA identifier, avoiding unsuitable selection and delivering a rapid response. The Rung Kutta approach is used to construct the proposed online identifier, which acts as the MG model. To imitate the frequency response of the MG online, the AOA predicts the coefficients of the online identifier based on the MG's input and output. Based on the online AOA identifier coefficients, the AOA is used to regulate the inertia and damping coefficients of the VIC. The effectiveness of the proposed explicit adaptive modified VIC is then evaluated in comparison to the conventional VIC based on the fixed parameters used in [31], the VIC system based on optimal parameters using AOA offline, and the adaptive VIC system based on fuzzy logic control [25] under mutation in loads, weather-dependent input, and MG parameters using MATLAB /Simulink software. The results highlight enhanced frequency stability and demonstrate the efficiency of the proposed explicit adaptive modified VIC in accommodating low-inertia islanded MGs with RESs and load fluctuations.

The remainder of the paper is structured as follows: Section 2 explains the mathematical structure of MG. Section 3 depicts the proposed explicit adaptive VIC technique based on an online AOA identification. Section 4 gives the simulation results and a discussion. Section 5 presents the conclusion.

2. Overview of an Islanded Microgrid System

In this study, the proposed online AOA identifier controlled adaptive modified VIC was investigated with the islanded MG studied, which has a system base of 15 MW which incorporates 15 MW TPP, 8.5 MW WPP, 4.5 MW SPP, 5 MW residential load, 10 MW industrial load, and 4.5 MW ESS, as shown in Figure 1. Table 1 shows the values of the MG parameters [36].

Variations in wind, load, and solar power are considered system disturbances. For valve gate opening and shutting, the generating rate constant (GRC) and rate limiter are incorporated into the exact perception of the MG.

On MG frequency deviation, primary, secondary (i.e., LFC), and inertia controls have the following effects:

$$\Delta f = \frac{1}{2Hs + D}(\Delta P_{TPP} + \Delta P_{WPP} + \Delta P_{SPP} + \Delta P_{ESS-Inertia} - \Delta P_d) \quad (1)$$

where

$$\Delta P_{TPP} = \frac{1}{1 + sT_T}(\Delta P_G) \quad (2)$$

$$\Delta P_G = \frac{1}{1 + sT_G}\left(\Delta P_C - \frac{1}{R}\Delta f\right) \quad (3)$$

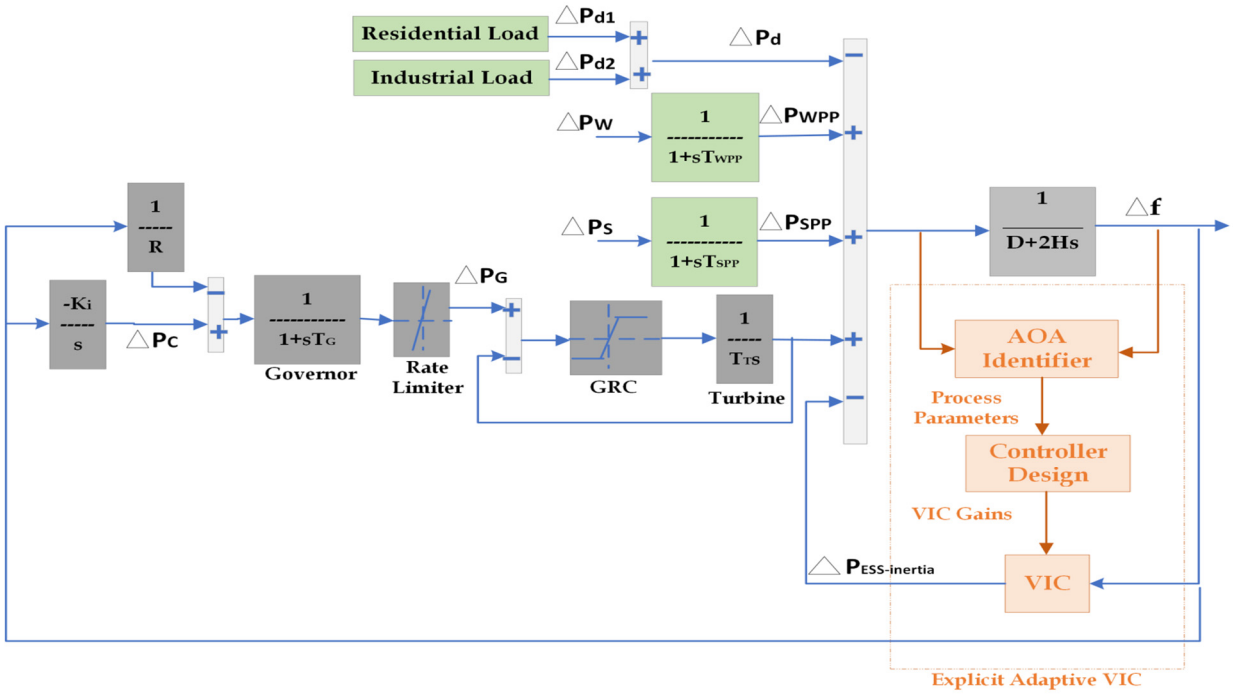

Figure 1. Block diagram of the Microgrid studied with the proposed online AOA identifier controlled adaptive modified VIC.

Table 1. Parameters of the studied MG [36].

Parameter	Value
Microgrid damping coefficient, D (p.u. MW/Hz)	0.016
Equivalent inertia constant, H (p.u. MWs)	0.082
Governor time constant, T_G (s)	0.100
Turbine time constant, T_T (s)	0.400
Wind turbine time constant, T_{WPP} (s)	1.500
Solar system time constant, T_{SPP} (s)	1.800
Speed droop characteristic, R (Hz/p.u.MW)	2.400
Integral control variable gain, KI (s)	−0.050
Virtual inertia control gain, K_{Hv} (s)	1.600
Virtual damping gain, K_{Dv} (s)	1.200
Virtual inertia time constant, T_{BESS} (s)	10.000
Maximum limit of valve gate, V_U (p.u. MW)	0.300
Minimum limit of valve gate, V_L (p.u. MW)	−0.300
Generation rate constraints, GRC (%)	20%
Frequency, f (Hz)	50.000

$$\Delta P_{WPP} = \frac{1}{1 + sT_{WPP}}(\Delta P_W) \tag{4}$$

$$\Delta P_{SPP} = \frac{1}{1 + sT_{SPP}}(\Delta P_S) \tag{5}$$

$$\Delta P_{ESS-Inertia} = \frac{K_{Hv}}{1 + sT_{BESS}}\left[\frac{d(\Delta f)}{dt}\right] \tag{6}$$

state vector,

$$X^T = \begin{bmatrix}\Delta f & \Delta P_G & \Delta P_{TPP} & \Delta P_{WPP} & \Delta P_{SPP} & \Delta P_{ESS-Inertia}\end{bmatrix} \tag{7}$$

disturbance input vector,

$$W^T = \begin{bmatrix}\Delta P_W & \Delta P_S & \Delta P_d\end{bmatrix} \tag{8}$$

As a result, the following covers the overall state-space representation of the MG considering RESs and ESS:

$$\dot{X} = \begin{bmatrix} -\frac{D}{2H} & 0 & \frac{1}{2H} & \frac{1}{2H} & \frac{1}{2H} & \frac{1}{2H} \\ -\frac{1}{RT_G} & -\frac{1}{T_G} & 0 & 0 & 0 & 0 \\ 0 & \frac{1}{T_T} & -\frac{1}{T_T} & 0 & 0 & 0 \\ 0 & 0 & 0 & -\frac{1}{T_{WPP}} & 0 & 0 \\ 0 & 0 & 0 & 0 & -\frac{1}{T_{SPP}} & 0 \\ \frac{-K_{Hv}*D}{T_{ESS}*2H} & 0 & \frac{K_{Hv}}{T_{ESS}*2H} & \frac{K_{Hv}}{T_{ESS}*2H} & \frac{K_{Hv}}{T_{ESS}*2H} & \left(\frac{K_{Hv}}{T_{ESS}*2H} - \frac{1}{T_{ESS}}\right) \end{bmatrix} * \begin{bmatrix} \Delta f \\ \Delta P_G \\ \Delta p_{TPP} \\ \Delta p_{WPP} \\ \Delta P_{SPP} \\ \Delta P_{Inertia} \end{bmatrix} + \begin{bmatrix} 0 \\ \frac{1}{T_G} \\ 0 \\ 0 \\ 0 \\ 0 \end{bmatrix} * [\Delta P_C] + \begin{bmatrix} 0 & 0 & -\frac{1}{2H} \\ 0 & 0 & 0 \\ 0 & 0 & 0 \\ \frac{1}{T_{WPP}} & 0 & 0 \\ 0 & \frac{1}{T_{SPP}} & 0 \\ 0 & 0 & -\frac{K_{Hv}}{T_{ESS}*2H} \end{bmatrix} * \begin{bmatrix} \Delta P_W \\ \Delta P_S \\ \Delta P_d \end{bmatrix} \quad (9)$$

$$Y = \begin{bmatrix} 1 & 0 & 0 & 0 & 0 & 0 \end{bmatrix} * X \quad (10)$$

3. The Proposed Online AOA Identifier-Controlled Adaptive Modified Virtual Inertia Control

3.1. Concept of Virtual Inertia Control

An MG's frequency diverges from its nominal value when a disturbance is applied because the disturbance creates a power imbalance. A power system performs several control procedures over a long period to sustain power generation and load balance. Initially, the primary frequency control (governor) minimizes the MG's frequency variation within the first few seconds. The automatic generation control (secondary control) returns the nominal value of the frequency within minutes. The reserve control action addresses current or anticipated MG disruptions [38]. Until the primary frequency control is enabled, the kinetic energy stored in the rotors counteracts this imbalance through inertial reaction. The initial 10 s of using RP sources result in a poor inertial response, which causes a rapid RoCoF and a significant frequency variation [39]. As a result, a low inertia MG may cause the tripping of frequency relays, load-shedding, or cascade outages [38]. The injection of synthetic or VI into MGs with low inertia is required to alleviate this problem. Inertia is the term used to describe the kinetic energy stored in rotational motion, and it is calculated as follows:

$$E_{KE} = \frac{1}{2} J\omega^2 \quad (11)$$

where J stands for the MG's inertia, and the angular frequency is denoted by ω. The swing equation can be used to roughly determine how a frequency disturbance will impact a power system's frequency:

$$P_G - P_d = \frac{dE_{KE}}{dt} = J\omega\frac{d\omega}{dt} \quad (12)$$

where the generated power and the power demand, including losses, are denoted by P_G, and P_d, respectively.

The power system's inertia constant H equals the kinetic energy of the connected generators in the system, normalized to apparent power S_g:

$$H = \frac{E_{KE}}{S} = \frac{J\omega^2}{2S}$$

$$H = \frac{J\omega_g^2}{2S_g} \quad (13)$$

Equation (12) can be written as follows:

$$\frac{2H}{\omega}\frac{d\omega}{dt} = \frac{(P_G - P_d)}{S} \quad (14)$$

by substituting the frequency, f, for the angular frequency,

$$\frac{2H}{f}\frac{df}{dt} = \frac{(P_G - P_d)}{S} \quad (15)$$

where $\frac{df}{dt}$ is the RoCoF of the system. As a result, by changing the power imbalance over a brief time, determining and reducing RoCoF is the main objective of such a VI imitation technique. Figure 2 depicts the structure of the proposed VIC (i.e., imitating both damping and inertia features). In comparison to conventional VI control methods (i.e., imitating only the inertia feature), a graphic representation of the presented methodology's effects on response time, steady-state error, and damping is shown in Figure 3, including speedy response, reduced steady-state error, and improved damping. The online AOA optimization algorithm has been applied in the proposed explicit adaptive VIC system to choose the appropriate values for K_{Dv} and, K_{Hv} while taking into consideration the dynamically changing variables of the MG. The structures of the online identifier for MG, as well as the proposed explicit VIC, are described in the following sections.

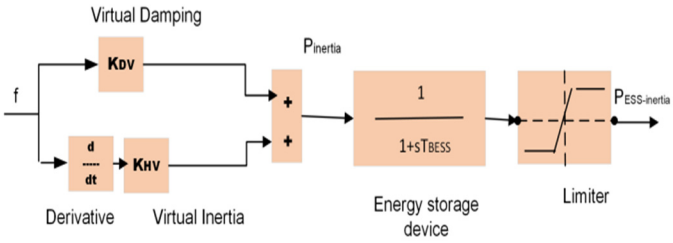

Figure 2. VIC Structure [31].

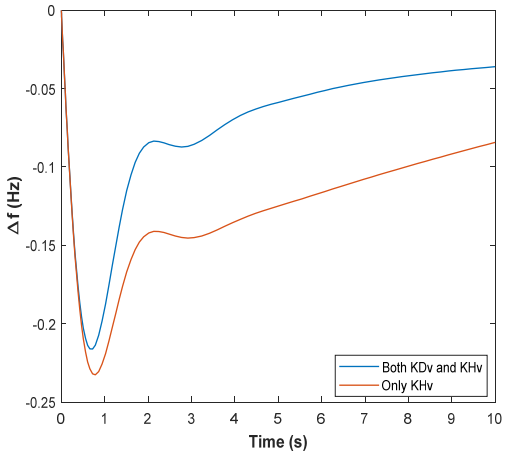

Figure 3. Effect of K_{Dv} and K_{Hv}.

3.2. Overview of Archimedes Optimization Algorithm (AOA) [40]

The AOA simulates what happens when weights and volumes of matter are submerged in a liquid using a population-based method. The weight of the liquid that the matter has displaced is applied to it as an upward force (a buoyant force), as shown in Figure 4.

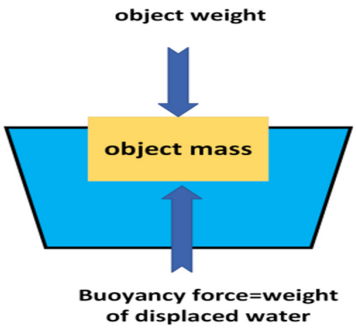

Figure 4. A matter is submerged in a liquid [40].

Assume that there are several matters submerged in the same liquid, as shown in Figure 5, each of which is attempting to reach equilibrium. Varied densities and volumes of submerged matter create different accelerations. The matter will be in balance if the buoyant force F_b and weight W_0 are equal.

$$F_b = W_o$$

$$p_b v_b a_b = p_o v_o a_o \tag{16}$$

$$a_o = \frac{p_b v_b a_b}{p_o v_o} \tag{17}$$

where the density, volume, and gravity or acceleration are denoted by p, v, and a, respectively. Liquid and submerged matter are indicated by the subscripts b and o, respectively.

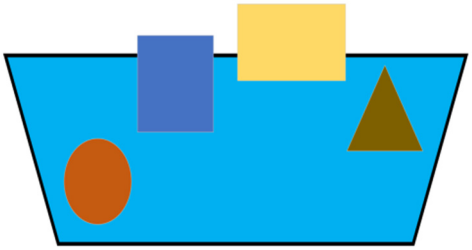

Figure 5. Several matters are submerged in the same liquid [40].

If the matters collide with each other (r), the following equilibrium condition results:

$$F_b = W_o$$

$$W_b - W_r = W_o$$

$$p_b v_b a_b - p_r v_r a_r = p_o v_o a_o \tag{18}$$

AOA begins the search with a random population of matters with different positions in liquid, volumes, densities, and accelerations. Once the beginning population's fitness has been assessed, the iteration procedure is continued until the dismissal condition is satisfied. AOA modifies the density and volume of each matter during each iteration.

Whether or not the matter collides with any other surrounding matter affects acceleration. The revised volume, acceleration, and density are used to establish a matter's new position. Below is a thorough mathematical expression of the AOA phases:

Step 1: For each ith matter, the position, volume (vol), density (den), and acceleration (acc) of all the matters are set to their initial values using the following formula:

$$x_i = lb_i + rand \times (ub_i - lb_i); i = 1, 2, \ldots N \tag{19}$$

The ith matter in a population of N matters is called x_i. lb_i and ub_i stand for the minimum and maximum boundaries of the search space, respectively.

$$den_i = rand, \quad vol_i = rand \tag{20}$$

where the D-dimensional vector (rand) produces a random number between [0, 1].

$$acc_i = lb_i + rand \times (ub_i - lb_i) \tag{21}$$

The matter is selected with the best fitness value after evaluating the first population. Allocate x_{best}, den_{best}, vol_{best}, acc_{best}.

Step 2: For iteration t + 1, the density and volume of matter i are changed as follows:

$$den_i^{t+1} = den_i^t + rand \times \left(den_{best} - den_i^t\right)$$

$$\mathrm{vol}_i^{t+1} = \mathrm{vol}_i^t + \mathrm{rand} \times \left(\mathrm{vol}_{best} - \mathrm{vol}_i^t\right) \tag{22}$$

where vol_{best} and den_{best} stand for the best matter's volume and density, and rand is a randomly generated number with a uniform distribution.

Step 3: After a period of time has passed since the first collision, the matter then seeks to attain equilibrium. The search is changed from exploration to exploitation, employing the transfer operator TF as follows:

$$\mathrm{TF} = \exp\left(\frac{t - t_{max}}{t_{max}}\right) \tag{23}$$

Hence, until the transfer TF crosses 1, it steadily rises. The iteration number and maximum iterations are denoted by t and t_{max}, respectively, In a similar way to how the density-decreasing factor d supports AOA when searching from a global to a local level. When using (24) over time, it becomes smaller:

$$d^{t+1} = \exp\left(\frac{t - t_{max}}{t_{max}}\right) - \left(\frac{t}{t_{max}}\right) \tag{24}$$

Hence, as time passes, d^{t+1} becomes smaller, permitting convergence in a predetermined appropriate area. AOA will balance between exploration and exploitation phases if this variable is handled properly.

Step 4:

(**Exploration phase**)**:** If matters collide with each other (TF $\leq$ 0.5), a random material (mr) is nominated and the matter's acceleration is adjusted for iteration t + 1 using:

$$\mathrm{acc}_i^{t+1} = \frac{\mathrm{den}_{mr} + \mathrm{vol}_{mr} \times \mathrm{acc}_{mr}}{\mathrm{den}_i^{t+1} \times \mathrm{vol}_i^{t+1}} \tag{25}$$

The density, volume, and acceleration of matter i are called den_i, vol_i, and acc_i, respectively. Moreover, using the subscript (mr) means the density, volume, and acceleration of random material. During one-third of iterations, TF $\leq$ 0.5 guarantees exploration. When a number other than 0.5 is used, the behavior of exploration and exploitation is altered.

(**Exploitation phase**)**:** If matters don't collide with each other (TF $>$ 0.5), the acceleration of matter is adjusted for iteration t + 1 as follows:

$$\mathrm{acc}_i^{t+1} = \frac{\mathrm{den}_{best} + \mathrm{vol}_{best} \times \mathrm{acc}_{best}}{\mathrm{den}_i^{t+1} \times \mathrm{vol}_i^{t+1}} \tag{26}$$

(**Normalization**)**:** the percentage of change is determined by normalizing the acceleration.

$$\mathrm{acc}_{i-norm}^{t+1} = u \times \frac{\mathrm{acc}_i^{t+1} - \min(\mathrm{acc})}{\max(\mathrm{acc}) - \min(\mathrm{acc})} + l \tag{27}$$

The normalization ranges u and l are adjusted to 0.9 and 0.1, respectively. The percentage change in each agent's step is specified by $\mathrm{acc}_{i,\,norm}^{t+1}$. If a matter's acceleration value is high and it is far from the global optimum, that matter i is in the exploration phase; if not, that matter i is in the exploitation phase. The acceleration factor often begins high and gradually decreases in usual cases. This enables search agents to steer clear of local solutions and toward the best global solution.

Step 5: The ith matter's position for iteration t + 1 during the exploration phase was determined by:

$$x_i^{t+1} = x_i^t + C_1 \times \mathrm{rand} \times \mathrm{acc}_{i-norm}^{t+1} \times d \times \left(x_{rand} - x_i^t\right) \tag{28}$$

where the constant $C_1 = 2$. If not, the following updates the positions of matters during the exploitation phase:

$$x_i^{t+1} = x_{best}^t + F \times C_2 \times rand \times acc_{i-norm}^{t+1} \times d \times \left(T \times x_{best} - x_i^t\right) \quad (29)$$

$$T = C_3 \times TF$$

$$F = \begin{cases} +1 \text{ if } P \leq 0.5 \\ -1 \text{ if } P > 0.5 \end{cases} \quad (30)$$

$$P = 2 \times rand - C_4$$

where the constant $C_2 = 6$. T grows with time in the interval $[C_3 \times 0.3,\ 1]$ and starts taking a percentage from the optimal position. Using the flag F alters the direction of motion.

Step 6: Determine the optimal solution path so far for each matter using the objective function f. Allocate x_{best}, den_{best}, vol_{best}, acc_{best}.

The working mechanism of the proposed AOA is illustrated in Figure 6.

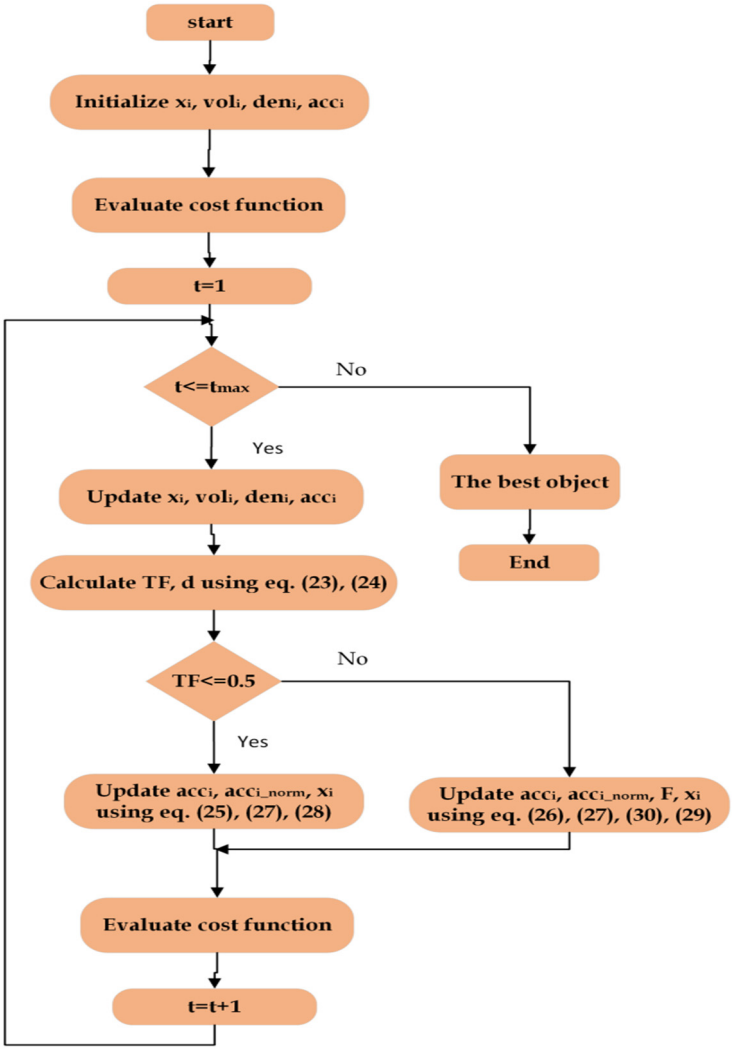

Figure 6. Flowchart of the AOA algorithm [40].

3.3. Structure of Explicit Self-Tuning Adaptive Control (ESTC)

The characteristics of the MG are being altered by the growing demand for renewable energy and will eventually be unknown. As a result, identification for a power system is now more frequently used. This study tended to use explicit self-tuning adaptive control,

which depends on the identification concept. As shown in Figure 7, explicit self-tuning adaptive control entails modeling, control law design, implementation, and validation. The "Identification" block, which acts as a model of the process (i.e., MG), is used to estimate the model parameters online. In this study, the online AOA identifier is chosen as a model of the MG. The controller design, which uses a specified approach, determines the controller parameters [13]. In this study, AOA was used to adjust online the parameters of VIC.

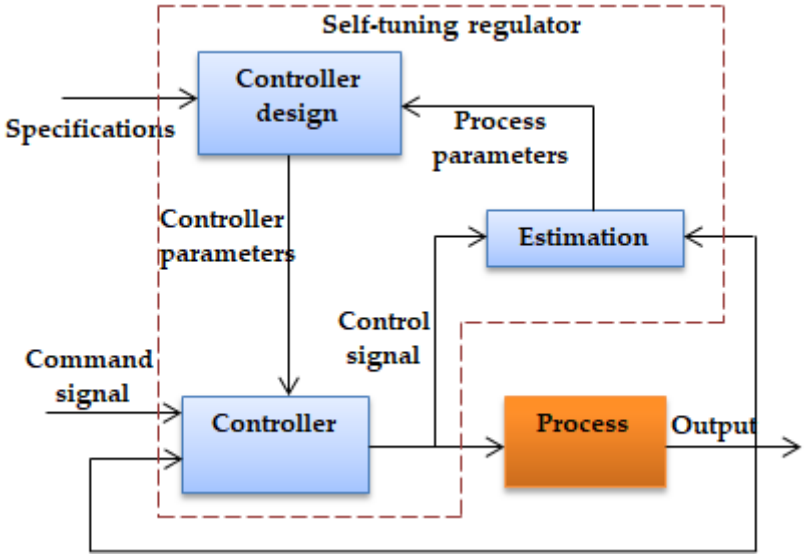

Figure 7. Block diagram of an explicit self-tuning regulator [13].

3.4. Structure of the Online AOA Identifier

The MG is considered to have a known model structure but unknown parameters. AOA is used to estimate online the changing values of parameters. The main concept is a comparison between the frequency output of the MG with the frequency output of the identifier. Through optimization, the difference between the MG and identifier output is reduced to a minimum using a fitness function. The fitness function is an indicator of convergence between the response of the identifier and the measured response of MG. The differential equation of the MG is as follows [41]:

$$\dot{x} = f(p, x, u)$$
$$y = g(p, x) \quad (31)$$

where f and g are linear or nonlinear functions, and p stands for the unknown parameter vector containing the inertia and damping coefficients of the MG (H,D) that will be determined. The differential equation of the identified model of the MG is as follows [41]:

$$\dot{\hat{x}} = f(\hat{p}, \hat{x}, u)$$
$$\hat{y} = g(\hat{p}, \hat{x}) \quad (32)$$

where the same MG input that was used to feed the MG model is u, and $\hat{p}$ is the estimated parameter vector which contains the identified inertia and damping coefficients of the identified model $(\hat{H}, \hat{D})$. The structure of the identified model is represented as the MG structure (31) using the Rung Kutta method (Appendix A). The MG input, MG response, and estimated coefficients are used to determine the response of the identified model. The difference between the responses of the MG y and the identified model $\hat{y}$ is used to evaluate the estimated parameters. Therefore, the definition of the fitness function is:

$$J = y - \hat{y} = \Delta f - \Delta \hat{f} = e$$

The fitness function depends on the estimated parameter vector, $\hat{p}$. Next, the identification challenge considers a problem of optimization. Figure 8 shows the AOA construction depending on the parameter identification approach online. First, both the MG to be identified and the MG model receive the MG input, u. Then, the performance evaluator generates the fitness function J using the output from the MG and its model. The AOA-based identifier identifies the unknown parameter vector $\hat{p}$ (i.e., $\hat{H}, \hat{D}$) using the calculated fitness function J. At every sampling time, the iteration number reaches a maximum, after which the estimated parameters $\hat{p}$ (i.e., $\hat{H}, \hat{D}$) update the MG model. The obtained value of $\hat{p}$ at this moment is considered to be the initial value for the next sampling time to reduce the number of iterations, and reach the optimum values of the AOA identifier achieved for the fitness function quickly. Table 2 gives the values of the online AOA parameters.

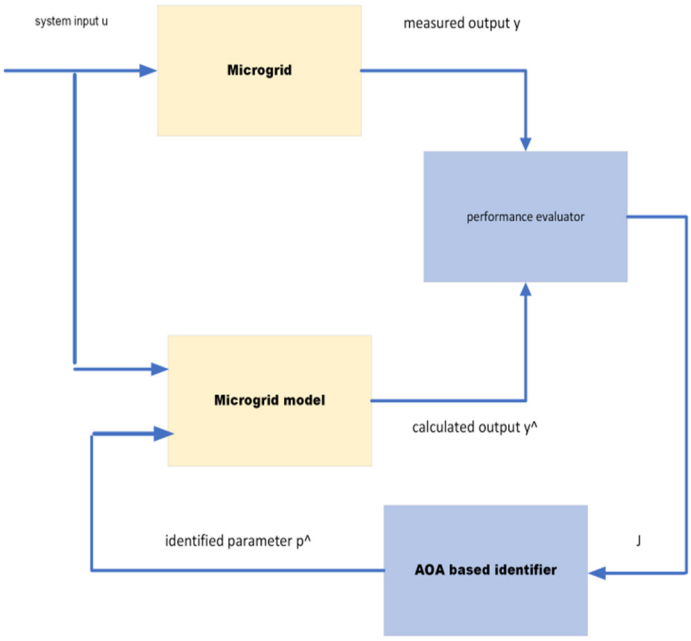

Figure 8. Block diagram of the online AOA identifier [41].

Table 2. Values of the online AOA identifier parameters.

Parameters	Value	Parameters	Value
C_1	2	C_4	0.5
C_2	6	t_{max}	7
C_3	2	N	5
H, D	[0, 0.1]		

3.5. The Proposed Explicit Adaptive Modified Virtual Inertia Control

Figure 9 shows a reduced representation of the MG, taking into consideration the VIC system. In Figure 10, G(s) represents the linearized transfer function of the MG studied without the VIC loop, as shown in Figure 9. Furthermore, H(s) represents the transfer function of the VIC, as shown in Figure 9, which acts as the feedback controller. Then, the transfer function of the closed loop of the MG with the VIC will be:

$$TF(s) = \frac{G(s)}{1 + G(s)H(s)}$$

where G(s) represents the power system transfer function and H(s) represents the feedback transfer function.

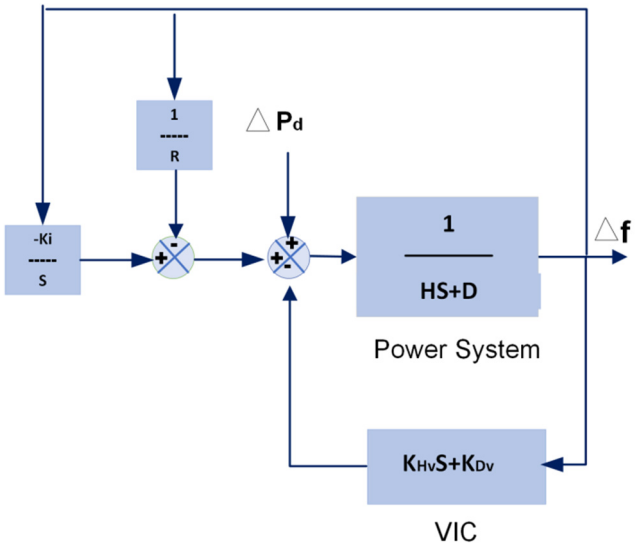

Figure 9. Reduced representation of the MG considering the VIC.

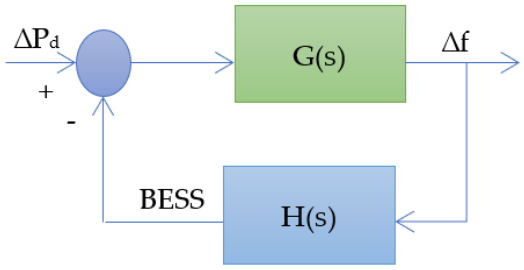

Figure 10. Block diagram of the closed loop of reduced MG considering the VIC.

From Figure 9:

$$G(s) = \frac{1}{HS + D\prime}\, H(s) = K_{Hv}S + K_{Dv} + \frac{K_i}{S} + \frac{1}{R}$$

Therefore, the following formula can determine the parameters of a closed-loop second-order system:

$$T.F = \frac{\omega_n^2}{S^2 + 2\eta\omega_n S + \omega_n^2} \tag{33}$$

the characteristic equation of a closed-loop second-order system will be:

$$1 + G(s)H(s) = S^2 + 2\eta\omega_n S + \omega_n^2 = 0 \tag{34}$$

$$1 + \left(\frac{1}{HS + D}\right)\left(K_{Hv}S + K_{Dv} + \frac{K_i}{S} + \frac{1}{R}\right) = 0$$

$$S^2 + \left(\frac{D + K_{Dv} + \frac{1}{R}}{H + K_{Hv}}\right)S + \left(\frac{K_i}{H + K_{Hv}}\right) = 0 \tag{35}$$

by substituting Equation (35) in Equation (34)

$$\omega_n = \sqrt{\frac{K_i}{H + K_{Hv}\prime}},\ \eta = \left(\frac{D + K_{Dv} + \frac{1}{R}}{H + K_{Hv}}\right)/2\omega_n, \tag{36}$$

However, Figure 11 explains the construction of the MG, taking into consideration the proposed online AOA identifier controlled explicit adaptive modified VIC. The Rung Kutta

approach, which depicts the structure of the identified model of the MG studied, uses AOA to determine its unknown parameters. Therefore, the AOA identifier estimates the inertia and damping coefficients of the identified model of the MG ($\hat{H}, \hat{D}$) online according to the measured input and the MG output, whereas, AOA updates online the values depending on the objective function, which is the difference between the MG output and the identifier output. With the optimum values of the inertia and damping coefficients ($\hat{H}, \hat{D}$), the AOA identifier acts as a model for the MG studied (i.e., the output of the AOA identifier should mimic the frequency deviation of the MG studied). The controller design uses AOA to achieve online the optimum values of the VIC gains (i.e., inertia K_{Hv} and damping K_{Dv} features) based on the identified coefficients ($\hat{H}, \hat{D}$). AOA initializes these gains values (K_{Hv}, K_{Dv}) with random values between 0 and 10. Table 3 shows the selection of the other parameters. AOA then updates online the initial values to achieve the objective function J, which is a function of the identified coefficients of the MG ($\hat{H}, \hat{D}$), and the VIC gains (K_{Hv}, K_{Dv}). Therefore, based on the AOA identifier's parameters, the following parameters can be derived for a closed-loop second-order system:

$$\omega_n = \sqrt{\frac{K_i}{\hat{H} + K_{Hv}}}\eta = \left(\frac{\hat{D} + K_{Dv} + \frac{1}{R}}{\hat{H} + K_{Hv}}\right)/2\omega_n, \tag{37}$$

$$T_r = \frac{\pi - \sqrt{(1-\eta^2)}}{\omega_n\sqrt{(1-\eta^2)}}, \; T_s = \frac{4}{\eta\omega_n}, \; M_P = e^{\frac{-\pi\eta}{\sqrt{(1-\eta^2)}}}$$

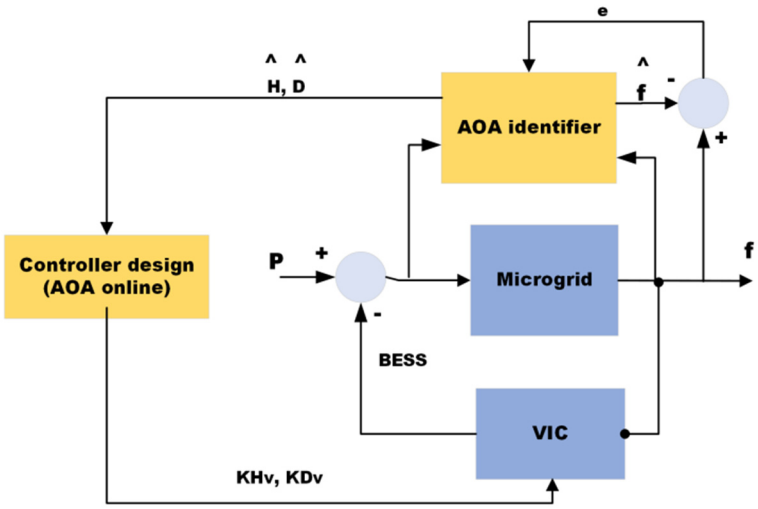

Figure 11. The MG with the proposed online AOA identifier controlled explicit adaptive modified VIC.

Table 3. The parameter values of online AOA controller design.

Parameters	Value	Parameters	Value
C_1	2	C_4	0.5
C_2	6	t_{max}	7
C_3	2	N	5
K_{Hv}, K_{Dv}	[0 10]		

The objective function J can be represented as follows:

$$J = \min\left(\sum T_r + T_s + M_P\right) \tag{38}$$

After the perfect values of the VIC gains have been obtained, the VIC gets these gains to reduce the frequency deviation during a system perturbation. Moreover, the current

values of gains are employed as initial values to launch the optimization approach at the next sampling time, to shrink the iteration numbers and save the MG stability and robustness. This approach is repeated at every sampling time to adjust the values of VIC gains, which improves the performance of MG faced with various load/RES disruptions.

4. Simulation Results and Discussion

Using the MATLAB/Simulink software, the frequency deviation of the proposed online AOA identifier controlled explicit adaptive modified VIC for the islanded MG was compared with the conventional VIC based on fixed parameters executed in [31], and the VIC system based on optimal parameters using AOA offline under various operational scenarios. Table 4 presents the parameter values of the AOA algorithm used to adjust the inertia and damping coefficients of VIC offline and the coefficient values of VIC.

Table 4. The Parameters Values of Offline AOA Algorithm and Coefficients Values of VIC.

Parameters	Value	Parameters	Value
C_1	2	t_{max}	100
C_2	6	N	5
C_3	2	K_{Hv}	7.5995
C_4	0.5	K_{Dv}	5.1842

4.1. First Scenario: Effect of Random Load Variation and Weather-Dependent Random Wind and Solar Power Variation

Using the nominal system characteristics shown in Table 1, the frequency response of the MG with the online AOA identifier controlled adaptive modified VIC was investigated in this scenario. The impact of fast and random variation in industrial and residential demand as well as in RES was employed to examine the frequency response of the proposed explicit adaptive modified VIC, as indicated in Figure 12.

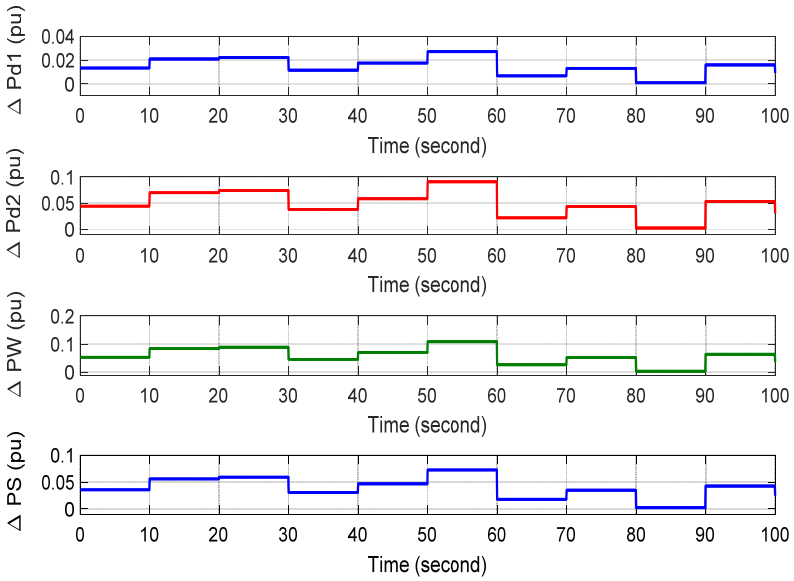

Figure 12. Variation in different penetration.

The online model identification based on the Rung Kutta method depended on the input and output of MG to mimic the MG response exactly. Moreover, as shown in Figure 13, the AOA modified the MG model coefficients (identified inertia and damping coefficients $\hat{H}, \hat{D}$) based on the variation between the MG and the identified model responses for every sampling instant.

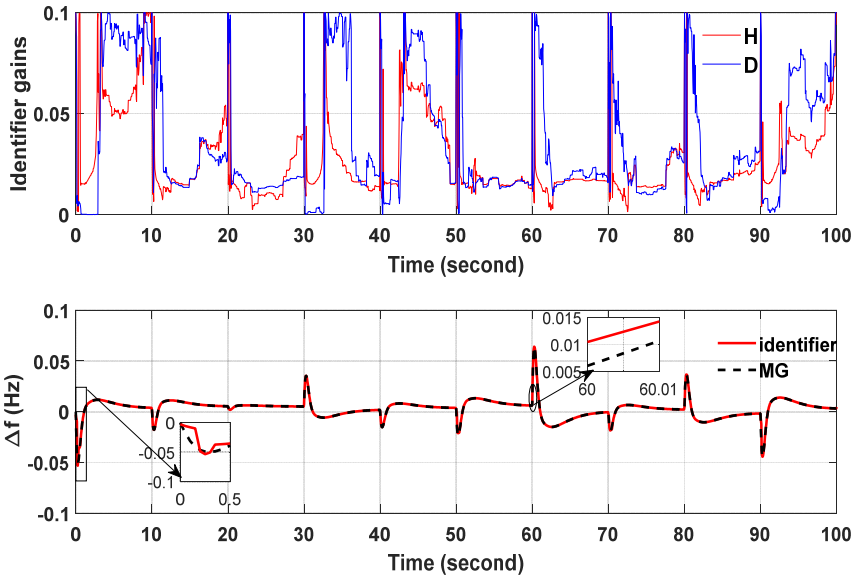

Figure 13. AOA identifier gains (virtual inertia and damping), and frequency response of the AOA.

In Figure 14, the dynamic response of the MG with the conventional VIC, the AOA optimized VIC offline, and the proposed explicit adaptive modified VIC are indicated under the influence of random perturbation. The frequency deviation of the MG oscillated between ±0.15 Hz and ±0.075 Hz with the conventional VIC and the AOA-optimized VIC offline, respectively. However, the MG response varied by about ±0.065 Hz as a result of the proposed explicit adaptive VIC. Therefore, it improved the MG performance in terms of speed, steady-state error, and damping. The proposed explicit adaptive VIC has a minimal steady-state error and is well-damped, even when subjected to large sudden changes of loads/renewables uncertainties at 60 s. On other hand, the proposed explicit adaptive VIC handled loads/renewables uncertainties.

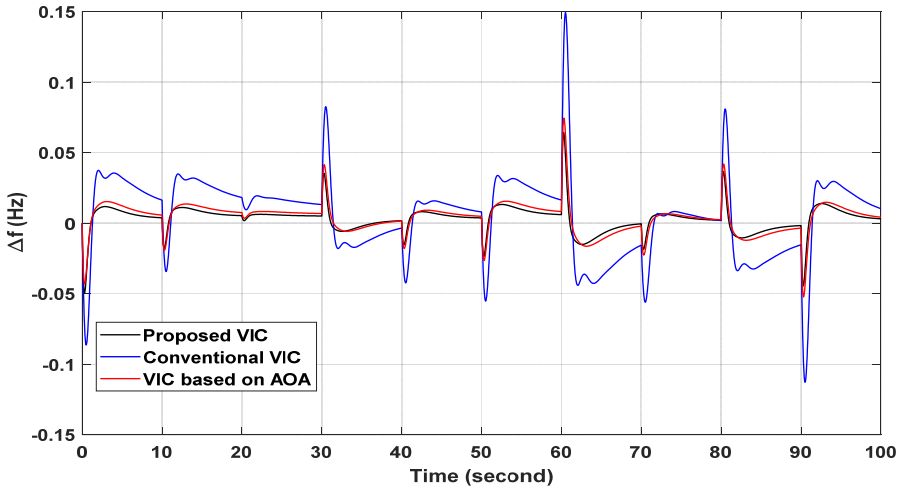

Figure 14. MG response.

Figure 15 explains the responses of the conventional VIC, the AOA-optimized VIC offline, and the proposed explicit adaptive VIC. The power response of BESS with the proposed explicit adaptive VIC injected a high degree of power into the MG at large system disturbances to overcome the effects of the physical constraints and system uncertainties.

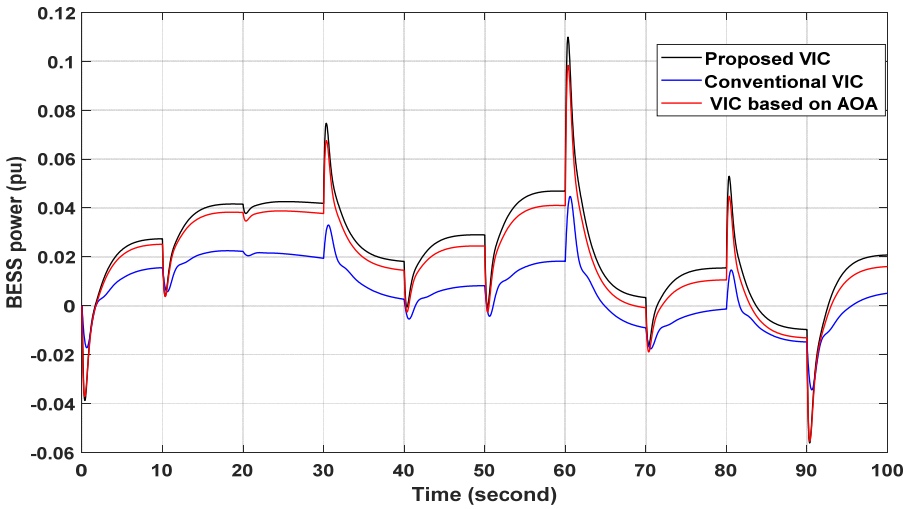

Figure 15. BESS power.

The AOA estimated online the VIC gains (inertia and damping coefficients), as shown in Figure 16, for every sampling instant. Furthermore, in every sampling instant, the AOA depended on the previous value of VIC gains as initial values for the current sampling instant. Therefore, these gains tended to settle and save the MG stability when different disturbances occurred. So, the proposed explicit adaptive VIC had the efficiency to robustly adjust the frequency in all meteorological and seasonal conditions, as well as during periods of peak and low load demand.

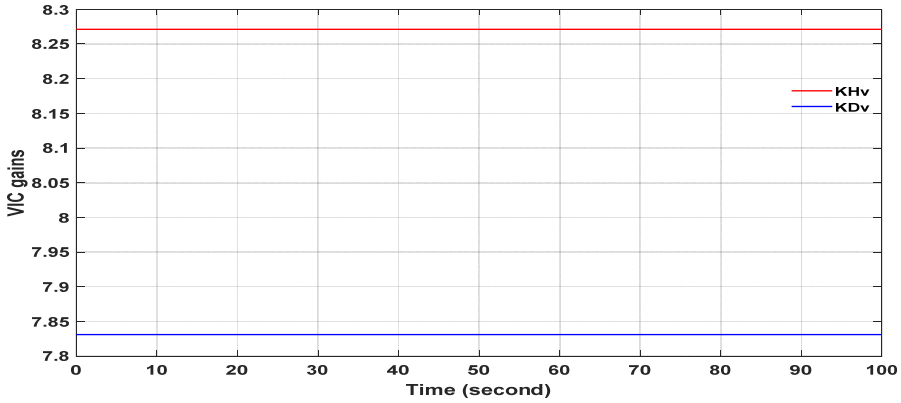

Figure 16. VIC gains.

4.2. Second Scenario: Effect of Various Operating Conditions

The frequency response of the proposed explicit adaptive modified VIC was surveyed under severe conditions. At 40 s, the residential load was cut off from the MG, and wind and solar power connected at the start time, whereas the industrial load connected at 20 s, as shown in Figure 17. The AOA adjusted online the parameters of the identifier ($\hat{H}$, $\hat{D}$) which acts as a model of the MG through time change. These parameters tended to steady state when the different disturbances ended. The AOA reached the best values of the parameters of the MG model. Therefore, the performance of the online AOA identifier was identical to the MG response, as illustrated in Figure 18.

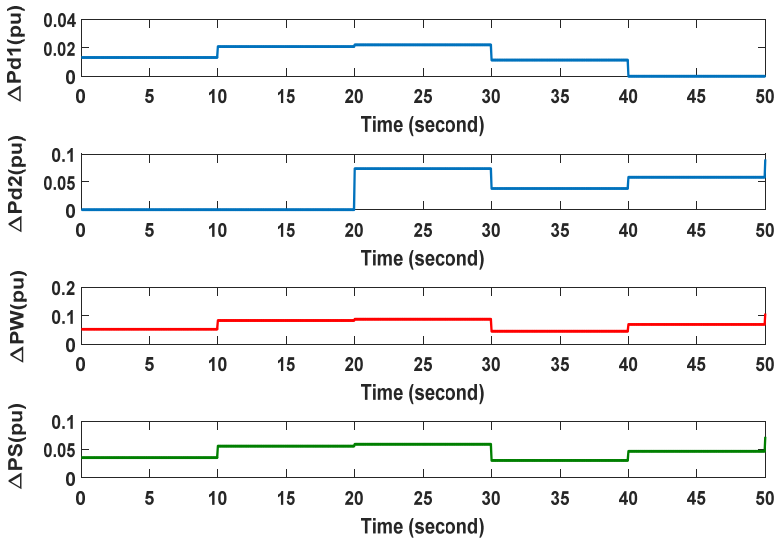

Figure 17. Variation in different penetration.

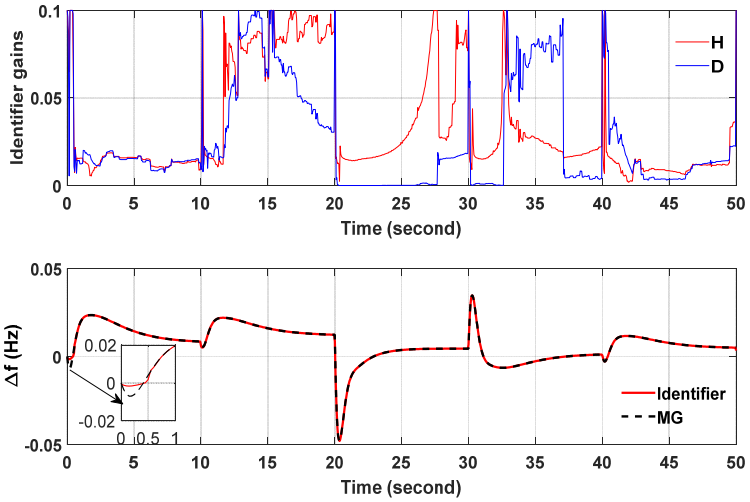

Figure 18. AOA identifier gains (virtual inertia and damping), and frequency response of the AOA identifier.

In Figure 19, the dynamic performance of the MG with the conventional VIC, the AOA optimized VIC offline, and the proposed explicit adaptive modified VIC are shown under severe conditions. The MG response varied between ±0.13 Hz and ±0.05 with conventional VIC and AOA-optimized VIC offline, respectively. However, with the proposed explicit adaptive modified VIC, the MG response fluctuated between ±0.035 Hz. As a result, it enhanced the MG's speed, steady-state error, and damping performance. Figure 20 depicts the reactions of the conventional VIC, the AOA-optimized VIC offline, and the proposed explicit adaptive modified VIC. The power reaction of the proposed explicit adaptive modified VIC is considered to be the best one. In Figure 21, the VIC gains (inertia and damping) are shown, where the AOA reached the optimum values of the gains at the first sampling instant and saved the optimum values for every sampling instant based on the previous value of VIC gains as initial values for the current sampling instant to improve the MG stability. Therefore, these gains tended to settle and save the MG stability when different disturbances occurred. So, the most robust and efficient control technique is the proposed explicit adaptive modified VIC.

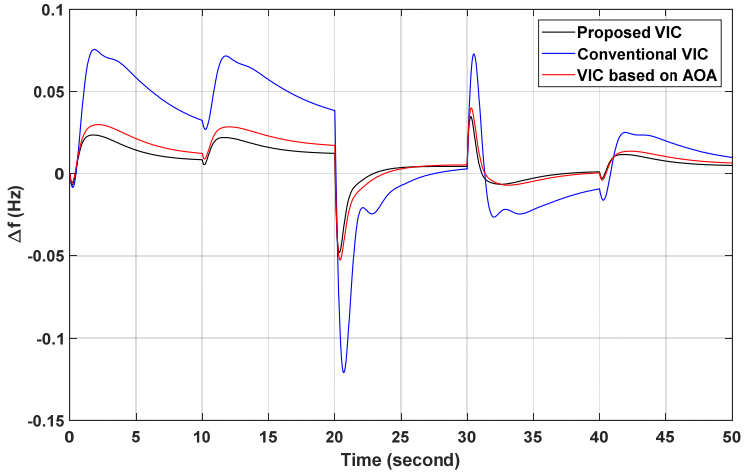

Figure 19. MG response.

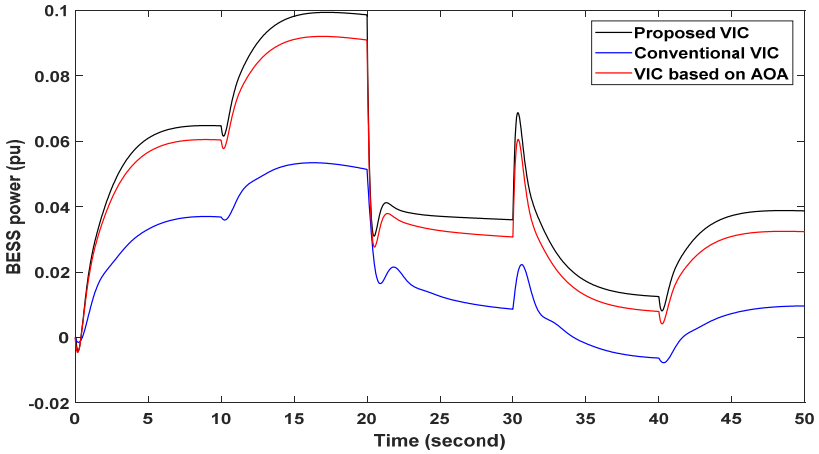

Figure 20. BESS power.

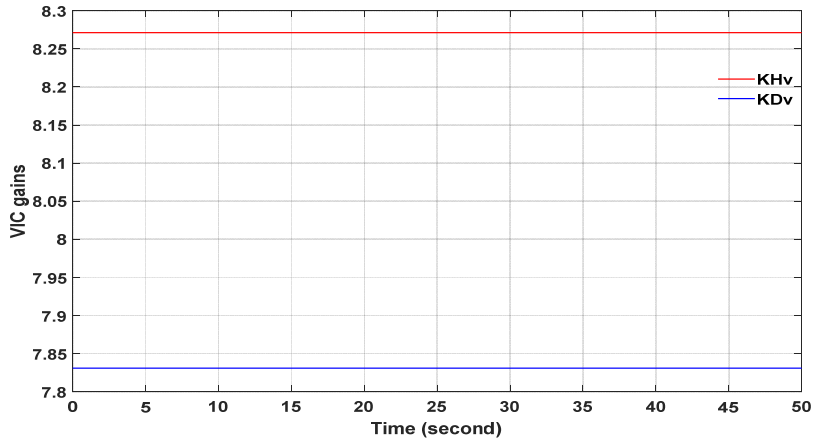

Figure 21. VIC gains.

4.3. Third Scenario: Effect of Various Operating Conditions with Low System Inertia

A reduction in the system's inertia to 75% of its nominal value occurred. Figure 22 represents the high integration of RESs and the 10% step load at 20 s. For every sampling instant, the gains of the online AOA identifier alternated. These gains tended to steady state when the different disturbances ended at 30 s. The AOA reached the best values of the parameters of the MG model($\hat{H}$, $\hat{D}$). So, the performance of the online AOA identifier

imitated the MG performance, as explained in Figure 23. In Figure 24, the efficiency of the proposed explicit adaptive modified VIC faced the high integration of RESs, step load, and variations of system parameters. In this case, a significant oscillation reached ±0.5 Hz with the conventional VIC. However, one oscillation decreased to ±0.2 Hz with the AOA-optimized VIC offline, and ±0.15 Hz with the proposed explicit adaptive VIC. To further the inertia reduction that took place, the BESS power increased with the proposed explicit adaptive modified VIC to counteract the effects of the physical constraints and system uncertainties, as illustrated in Figure 25. Figure 26 displays the VIC gains (inertia and damping coefficients). The AOA still attained the optimum values of the gains at the first sampling instant and saved MG stability, whereas the proposed approach was close to the global optima at every sampling instant. Figure 27 shows the speed convergence of the proposed approach with optimum value for four samples of consecutive instant times. This made the proposed explicit adaptive modified VIC a robust and effective control method. The significant dynamic response of the conventional VIC, the AOA-optimized VIC offline, and the proposed explicit adaptive modified VIC are all summarized in Figure 28.

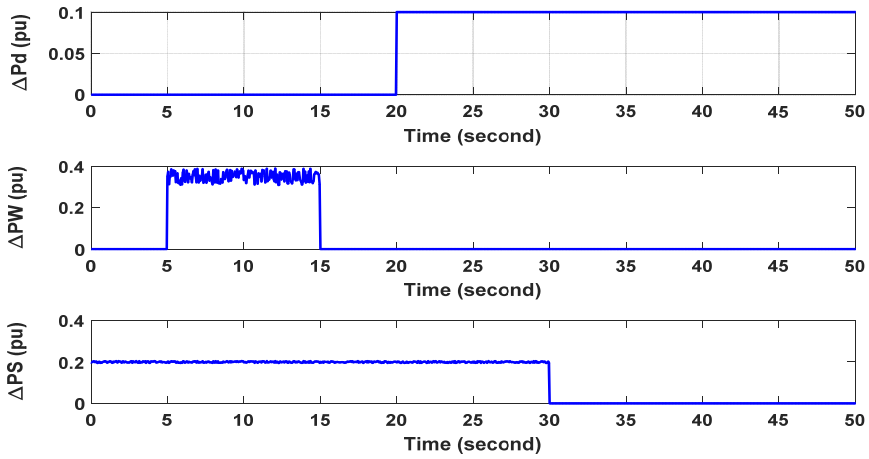

Figure 22. Variation in different penetration.

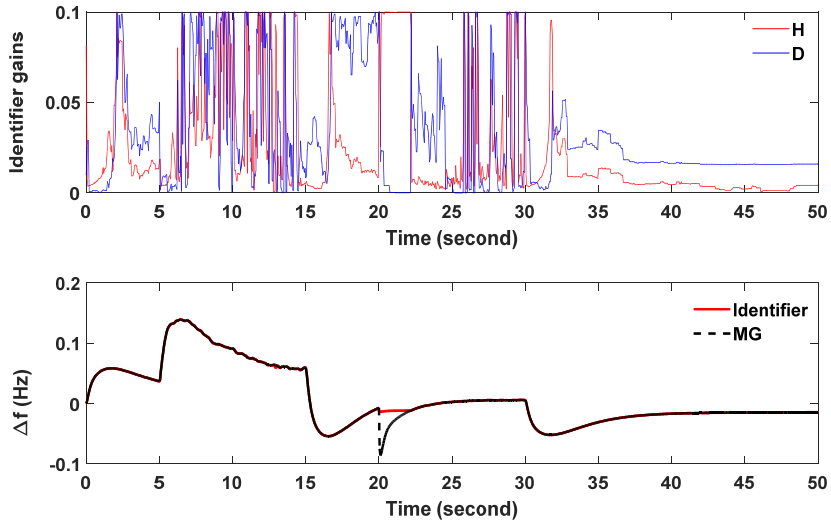

Figure 23. AOA identifier gains (virtual inertia and damping), and frequency response of the AOA identifier.

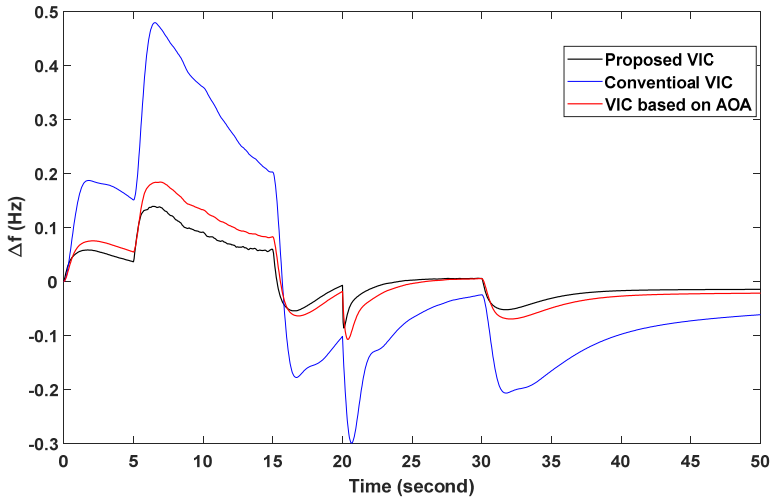

Figure 24. MG response.

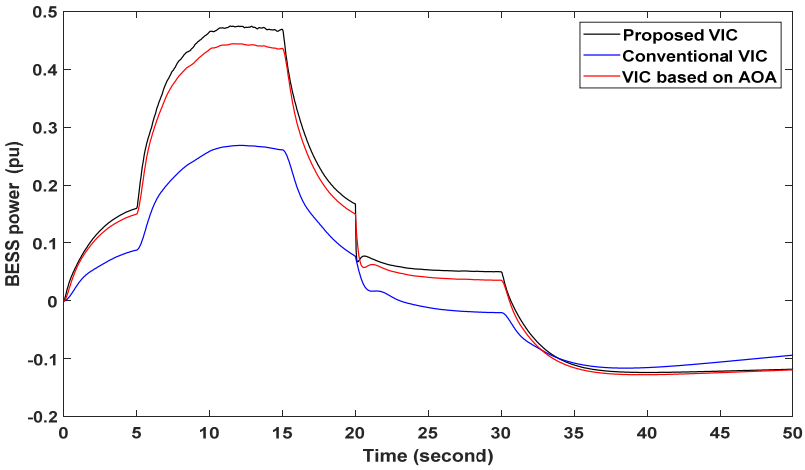

Figure 25. BESS power.

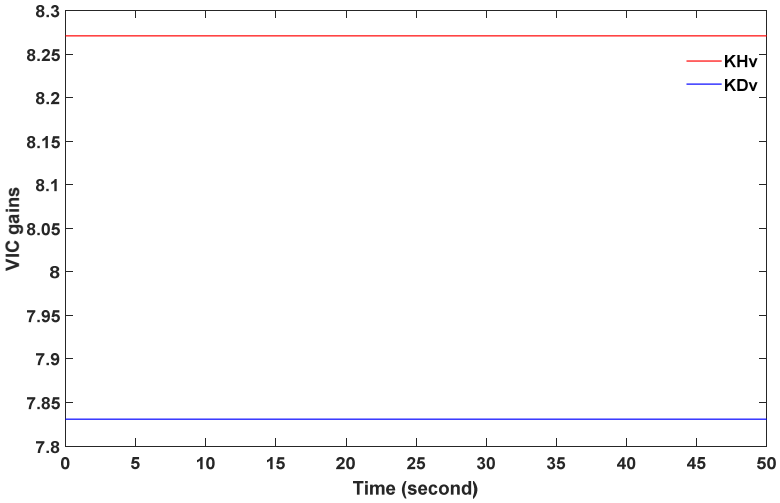

Figure 26. VIC gains.

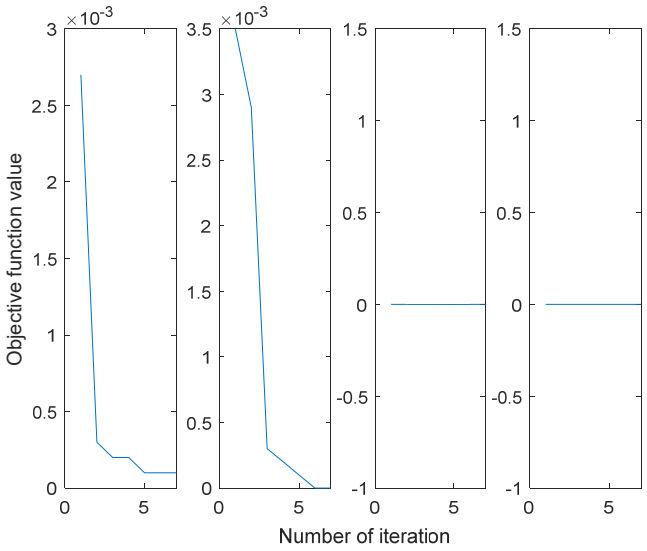

Figure 27. Speed convergence curves of the proposed controller at four consecutive instant times.

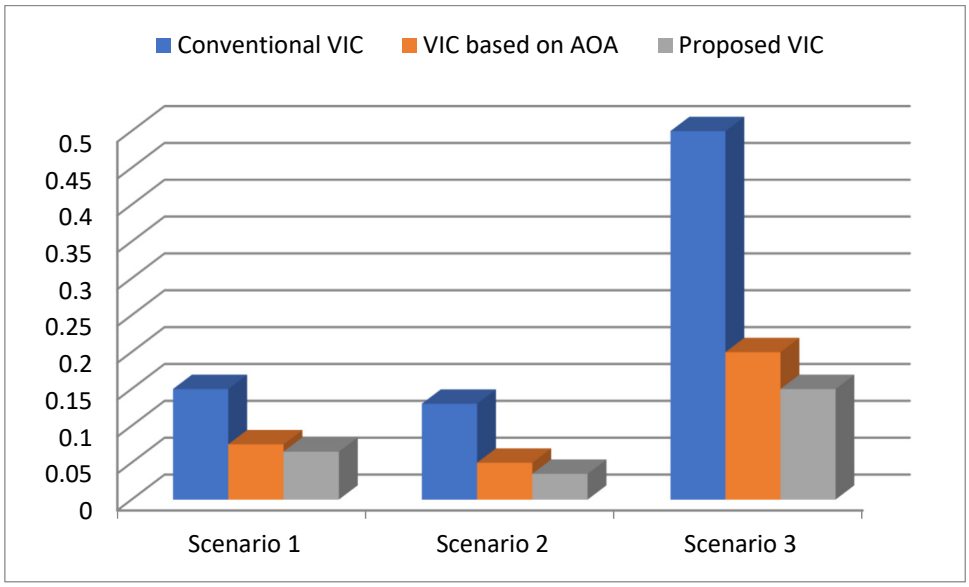

Figure 28. Maximum frequency deviation.

4.4. Effect of Variation in Various Parameters

Figure 29 shows the effect of the change of the computational parameters (i.e., H, D, T_g, T_t, T_W, T_S, R and K_i) on the proposed explicit adaptive modified VIC when $\Delta P_d = \Delta P_w = \Delta P_s = 0.1$ p.u. The frequency response of the MG with the proposed explicit adaptive modified VIC using the nominal system characteristics shown in Table 1 was compared when the value of the computational parameters was reduced by 50%. As a result, the proposed explicit adaptive modified VIC was slightly sensitive to the change of the time constant of the WPP (i.e., T_W) and the time constant of the SPP (i.e., T_S). The proposed explicit adaptive modified VIC then adjusted the frequency efficiently, despite the variation of parameters.

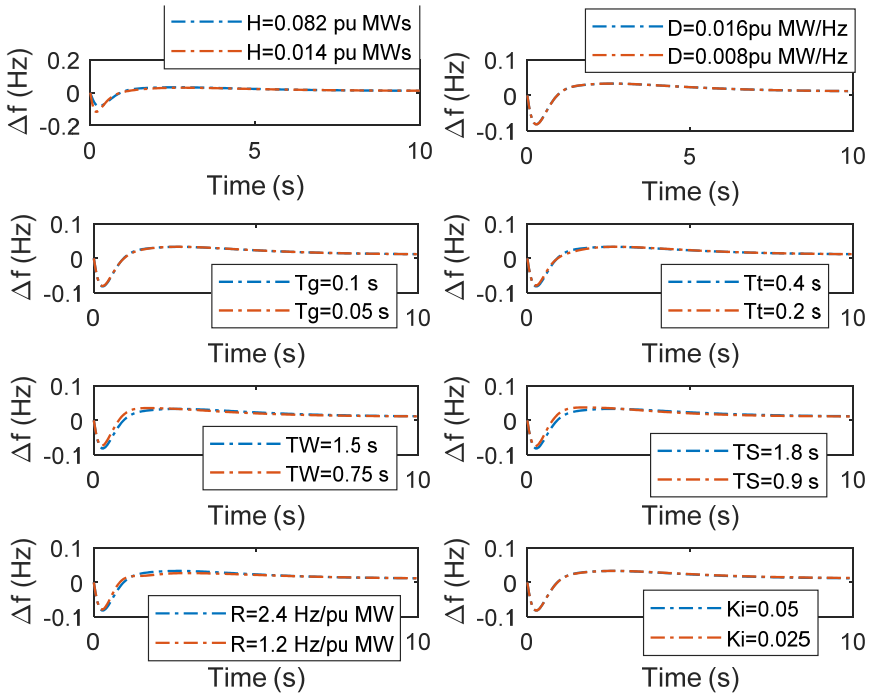

Figure 29. Sensitivity of the proposed VIC performance with the change of computational parameters.

4.5. Effectiveness Evaluation of The Proposed Explicit Adaptive VIC

An online AOA identifier controlled adaptive modified VIC was compared with the self-adaptive VIC-based fuzzy logic in [25] to validate its efficiency and robustness. Only the virtual inertia constant was automatically adjusted based on input signals of real power injection of RESs and system frequency deviations, as shown in Figure 30. The output was a normalized value of the virtual inertia constant. The fuzzy rule base in Table 5 was used to evaluate the suitable output depending on the input signals of ΔP_{RES} and Δf. The membership functions for the input and output of the fuzzy system are shown in Figure 31.

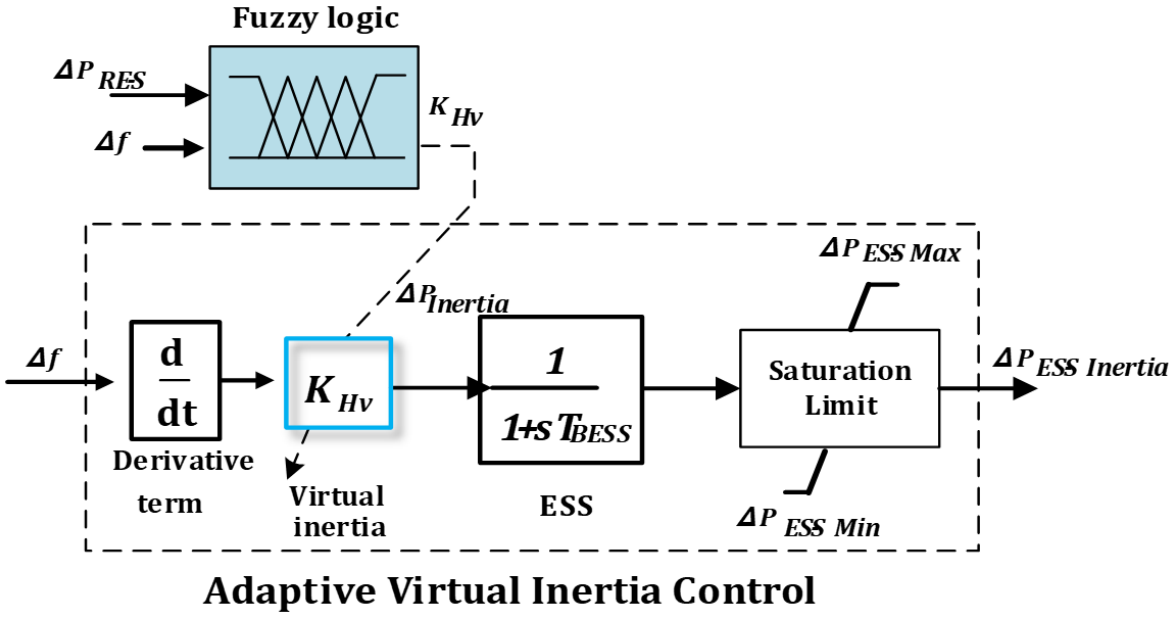

Figure 30. VIC-based fuzzy logic controller [25].

Table 5. Fuzzy rules of self-adaptive VIC for the linguistic variable [25].

		Δf				
		NL	**NS**	**ZO**	**PS**	**PL**
ΔP_{RES}	L	ZO	ZO	ZO	ZO	M
	M	S	S	M	B	B
	H	M	M	M	VB	VB

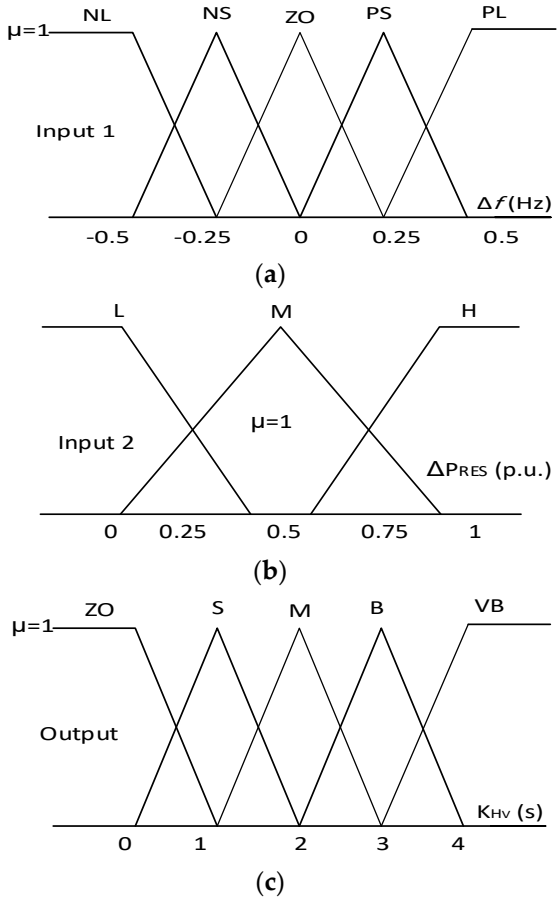

Figure 31. Symmetric fuzzy membership functions: (**a**) System frequency deviations. (**b**) RESs power changes/penetration. (**c**) Virtual inertia constant [25].

The input and output were divided into fuzzy subsets and defined using the linguistic variable. NL represents negative large, NS represents negative small, ZO represents zero, PS represents positive small, PL represents positive large, L represents low, M represents medium, H represents high, S represents small, B represents big, and VB represents very big.

In the third scenario, the frequency deviation of the MG based on the adaptive VIC-based fuzzy logic control was changed between ±0.6 Hz, as shown in Figure 32. However, one oscillation decreased to ±0.15 Hz with the proposed explicit adaptive VIC, which proves that the proposed explicit adaptive VIC is more robust and effective than the adaptive VIC-based fuzzy logic control. The BESS power increased with the proposed explicit adaptive modified VIC, as illustrated in Figure 33. Figure 34 displays the proposed explicit adaptive VIC gains (inertia and damping coefficients) and the inertia gain of the adaptive VIC-based fuzzy logic control, whereas the damping gain was neglected in [25]. The significant dynamic response of the VIC based on fuzzy logic control and the proposed explicit adaptive modified VIC are summarized in Figure 35. As a result, indirect adaptive controllers (i.e., the proposed explicit adaptive VIC) are considered more powerful than intelligent controllers (i.e., the adaptive VIC-based fuzzy logic control) in

reducing oscillations and enhancing power system stability, as mentioned before in the introduction section.

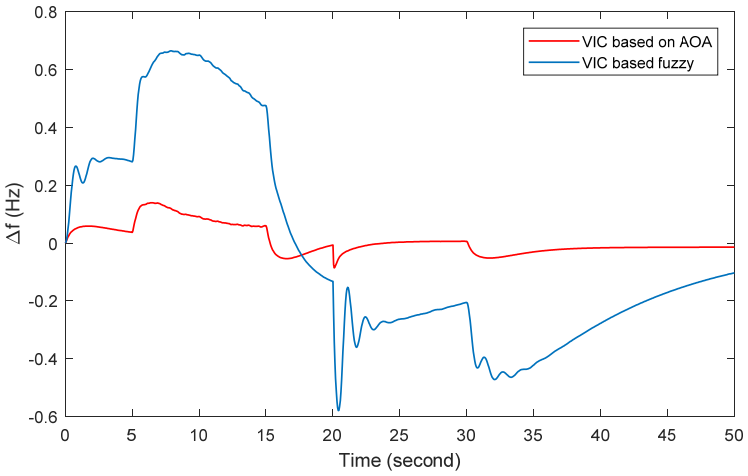

Figure 32. MG response.

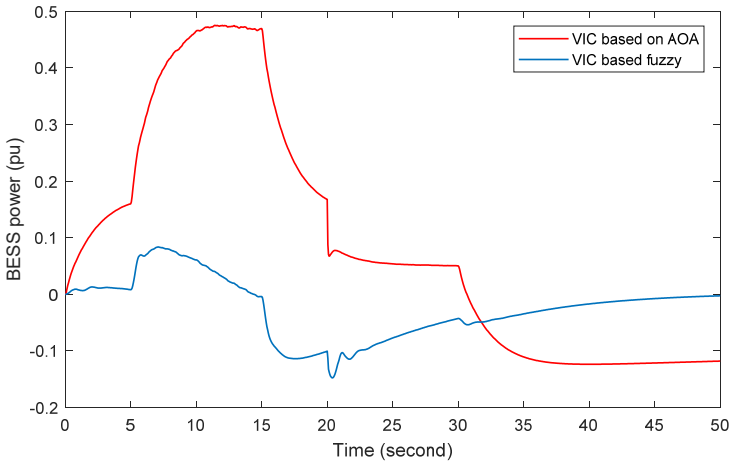

Figure 33. BESS power.

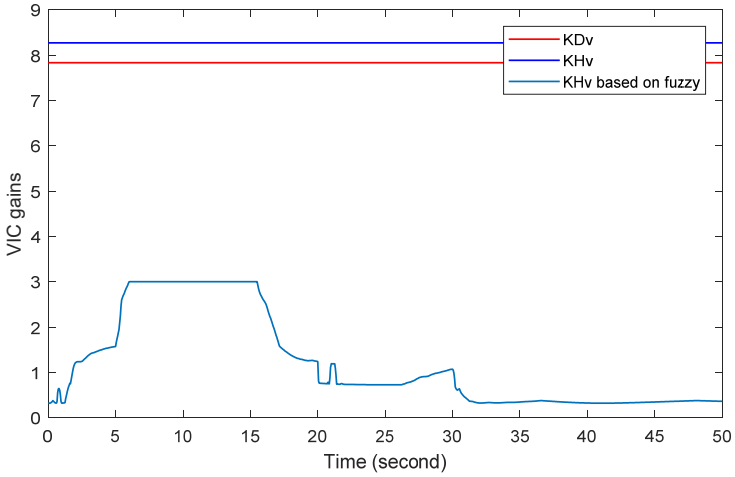

Figure 34. VIC gains.

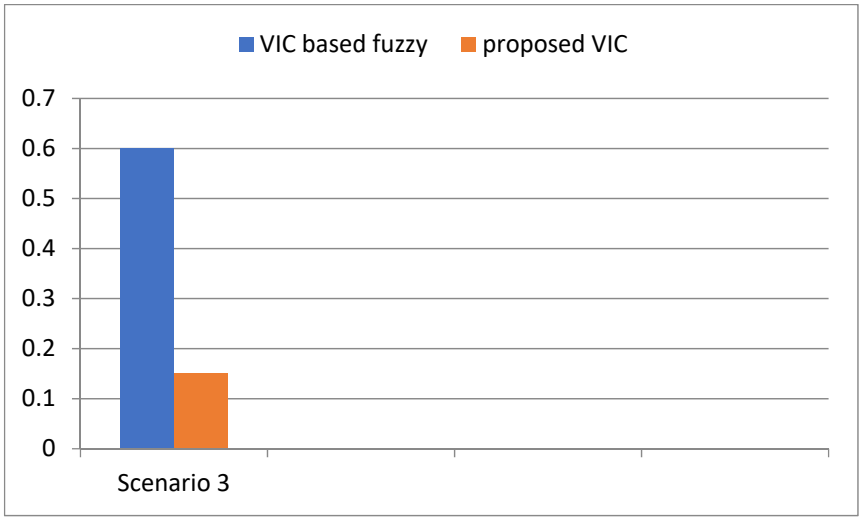

Figure 35. Maximum frequency deviation.

5. Conclusions

Widespread employment of renewable energy sources (RESs) reduces the inertia of the microgrid (MG). After this, frequency stability may regress as a result of power imbalance, minor load perturbation, or weather-dependent fluctuations. Most literature suggests that the design of virtual inertia control (VIC) systems rely on constant inertia and damping coefficient values, which may have a substantial impact on the frequency stability of microgrids at various levels of renewable energy penetration, where fixed values of virtual inertia and damping coefficients or inappropriate value selections may lead to higher frequency oscillations. To overcome such a problem, an explicit adaptive modified VIC is proposed. In this concept, the virtual inertia and damping coefficients are automatically adjusted using Archimedes optimization algorithm (AOA) based on an online AOA identifier, avoiding unsuitable selection and delivering a rapid response. An AOA identifier controlled adaptive modified VIC is suggested to boost the frequency stability of MG, which eliminates the effect of RESs oscillation, load variation, and dynamic perturbation (i.e., inertia and damping parameters of MG). The online AOA identifier assesses the coefficients of the MG at every sampling instant. The AOA then adjusts online the inertia and damping parameters of the VIC using the online coefficients of the MG. Using MATLAB /Simulink software, the simulation results demonstrate improved frequency stability, and the capabilities of the proposed explicit adaptive modified VIC to accommodate low-inertia islanded MGs with RESs and load fluctuations compared to conventional VIC based on fixed parameters, the VIC system based on optimal parameters using AOA offline, and the adaptive VIC system based on fuzzy logic control (i.e., estimate only the inertial gain). Therefore, in the simulation results, the battery energy storage system (BESS) should boost the microgrid with a high degree of power, which overcomes the effects of the physical constraints and system uncertainties. As a result, BESS should have a large power capacity, and this behavior may be affected BESS performance for a long time. In future studies, the other ESS may handle the expected problem.

Author Contributions: Conceptualization, A.F., M.G.H. and M.R.; Methodology, A.F. and Y.M.; Software, D.S.O. and M.G.H.; Validation, A.F.; Formal analysis, A.F., D.S.O., M.G.H. and M.R.; Investigation, Y.M., D.S.O., M.G.H. and M.R.; Writing—original draft, M.R.; Writing—review & editing, Y.M., D.S.O. and T.S.; Supervision, T.S.; Project administration, T.S.; Funding acquisition, T.S. All authors have read and agreed to the published version of the manuscript.

Funding: This research received no external funding.

Conflicts of Interest: The authors declare no conflict of interest.

Appendix A

Fourth-order Rung Kutta method [42].

The general formula giving the value of x for (n + 1) st step is

$$x_{n+1} = x_n + \frac{1}{6}(k1 + 2k2 + 2k3 + k4)$$

where

$$k1 = f(x_n,\ t_n)\Delta t \qquad k2 = f\left(x_n + \frac{k1}{2},\ t_n + \frac{\Delta t}{2}\right)\Delta t$$

$$k3 = f\left(x_n + \frac{k2}{2},\ t_n + \frac{\Delta t}{2}\right)\Delta t \qquad k4 = f(x_n + k3,\ t_n + \Delta t)\Delta t$$

The physical interpretation of the above solution is as follows:
k1 = (slope at the beginning of time step) Δt
k2 = (a first approximation to slope at midstep) Δt
k3 = (a second approximation to slope at midstep) Δt
k4 = (slope at the end of step) Δt

$$\Delta x = \frac{1}{6}(k1 + 2k2 + 2k3 + k4)$$

Thus Δx is the incremental value of x given by the weighted average of estimates based on slopes at the beginning, midpoint, and end of the time step.

References

1. Bevrani, H.; Ise, T.; Miura, Y. Virtual synchronous generators: A survey and new perspectives. *Int. J. Electr. Power Energy Syst.* **2014**, *54*, 244–254. [CrossRef]
2. Fang, J.; Li, H.; Tang, Y.; Blaabjerg, F. Distributed Power System Virtual Inertia Implemented by Grid-Connected Power Converters. *IEEE Trans. Power Electron.* **2018**, *33*, 8488–8499. [CrossRef]
3. Moghaddam, M.J.; Mojallali, H.; Teshnehlab, M. Recursive identification of multiple-input single-output fractional-order Hammerstein model with time delay. *Appl. Soft Comput.* **2018**, *70*, 486–500. [CrossRef]
4. Lugnani, L.; Dotta, D.; Lackner, C.; Chow, J. ARMAX-based method for inertial constant estimation of generation units using synchrophasors. *Electric Power Syst. Res.* **2020**, *180*, 106097. [CrossRef]
5. Shi, Y.; Hu, S.; Xu, D.; Su, J.; Liu, N.; Yang, X.; Du, Y. A simplified microgrid voltage and frequency response characteristic modeling method based on system identification. *Int. J. Electr. Power Energy Syst.* **2020**, *121*, 106063, ISSN 0142-0615. [CrossRef]
6. Ljung, L. *System Identification: Theory for the User*, 2nd ed.; Prentice-Hall: Hoboken, NJ, USA, 1998; Volume 19.
7. Bilal, B.; Hloindo Adjallah, K.; Sava, A.; Yetilmezsoy, K.; Kıyan, E. Wind power conversion system model identification using adaptive neuro-fuzzy inference systems: A case study. *Energy* **2022**, *239*, 122089, ISSN 0360-5442. [CrossRef]
8. Bakeer, A.; Magdy, G.; Chub, A.; Bevrani, H. A sophisticated modeling approach for photovoltaic systems in load frequency control. *Int. J. Electr. Power* **2022**, *134*, 107330. [CrossRef]
9. Elsaady, G.; Abd-El Meged Mohamed, A.H.; Fawzy, A. Self-tuning based on radial basis function neural network of a linear system. *Int. J. Sci. Eng. Res.* **2015**, *6*, 222–230.
10. Abd-Elmeged, M.; Gaber, E.; Ashraf, H.; Asmaa, F. Self-tuning DC servo motor design based on radial basis function neural network. *Int. J. Control Autom. Syst.* **2015**, *4*, 1–6.
11. Rashwan, A.F. An Indirect Self-Tuning Speed Controller Design for DC Motor Using a RLS Principle. In Proceedings of the 2019 21st International Middle East Power Systems Conference (MEPCON), Cairo, Egypt, 17–19 December 2019; pp. 633–638. [CrossRef]
12. Ramakrishna, G.; Malik, O.P. Adaptive PSS using a simple online identifier and linear pole-shift controller. *Electr. Power Syst. Res.* **2010**, *80*, 406–416. [CrossRef]
13. Rashwan, A.F.; Mahrous, A.; Mohamed, R.M.; Baha-El-Din, A.M.; Alkhalaf, S.; Senjyu, T.; Hemeida, A.M. Explicit adaptive power system stabilizer design based an on-line identifier for single-machine infinite bus. *Ain Shams Eng. J.* **2022**, *13*, 101544. [CrossRef]
14. Khooban, M.H.; Niknam, T.; Blaabjerg, F.; Dragičević, T. A new load frequency control strategy for micro-grids with considering electrical vehicles. *Electr. Power Syst. Res.* **2017**, *143*, 585–598. [CrossRef]
15. Brearley, B.J.; Prabu, R.R. A review on issues and approaches for microgrid protection. *Renew. Sustain. Energy Rev.* **2017**, *67*, 988–997. [CrossRef]
16. Hirase, Y.; Abe, K.; Sugimoto, K.; Sakimoto, K.; Bevrani, H.; Ise, T. A novel control approach for virtual synchronous generators to suppress frequency and voltage fluctuations in microgrids. *Appl. Energy* **2018**, *210*, 699–710. [CrossRef]

17. Rosewater, D.M.; Copp, D.A.; Nguyen, T.A.; Byrne, R.H.; Santoso, S. Battery Energy Storage Models for Optimal Control. *IEEE Access* **2019**, *7*, 178357–178391. [CrossRef]
18. Rakhshani, E.; Remon, D.; Cantarellas, A.M.; Garcia, J.M.; Rodriguez, P. Virtual Synchronous Power Strategy for Multiple HVDC Interconnections of Multi-Area AGC Power Systems. *IEEE Trans. Power Syst.* **2017**, *32*, 1665–1677. [CrossRef]
19. Rakhshani, E.; Remon, D.; Mir Cantarellas, A.; Rodriguez, P. Analysis of derivative control based virtual inertia in multi-area high-voltage direct current interconnected power systems. *IET Gener. Transm. Distrib.* **2016**, *10*, 1458–1469. [CrossRef]
20. Kerdphol, T.; Rahman, F.; Mitani, Y. Virtual Inertia Control Application to Enhance Frequency Stability of Interconnected Power Systems with High Renewable Energy Penetration. *Energies* **2018**, *11*, 981. [CrossRef]
21. Kerdphol, T.; Rahman, F.S.; Mitani, Y.; Watanabe, M.; Kufeoglu, S. Robust Virtual Inertia Control of an Islanded Microgrid Considering High Penetration of Renewable Energy. *IEEE Access* **2018**, *6*, 625–636. [CrossRef]
22. Ali, H.; Magdy, G.; Xu, D. A new optimal robust controller for frequency stability of interconnected hybrid microgrids considering non-inertia sources and uncertainties. *Int. J. Electr. Power Energy Syst.* **2021**, *128*, 106651. [CrossRef]
23. Chen, M.; Zhou, D.; Blaabjerg, F. Modelling, Implementation, and Assessment of Virtual Synchronous Generator in Power Systems. *J. Mod. Power Syst. Clean Energy* **2020**, *8*, 399–411. [CrossRef]
24. Moradi, M.H.; Amiri, F. Virtual inertia control in islanded microgrid by using robust model predictive control (RMPC) with considering the time delay. *Soft Comput.* **2021**, *25*, 6653–6663. [CrossRef]
25. Kerdphol, T.; Watanabe, M.; Hongesombut, K.; Mitani, Y. Self-Adaptive Virtual Inertia Control-Based Fuzzy Logic to Improve Frequency Stability of Microgrid with High Renewable Penetration. *IEEE Access* **2019**, *7*, 76071–76083. [CrossRef]
26. Kerdphol, T.; Rahman, F.S.; Watanabe, M.; Mitani, Y. Robust Virtual Inertia Control of a Low Inertia Microgrid Considering Frequency Measurement Effects. *IEEE Access* **2019**, *7*, 57550–57560. [CrossRef]
27. Nanda Kumar, S.; Mohanty, N.K. Modified Golden Jackal Optimization Assisted Adaptive Fuzzy PIDF Controller for Virtual Inertia Control of Micro Grid with Renewable Energy. *Symmetry* **2022**, *14*, 1946. [CrossRef]
28. Kerdphol, T.; Watanabe, M.; Mitani, Y.; Phunpeng, V. Applying Virtual Inertia Control Topology to SMES System for Frequency Stability Improvement of Low-Inertia Microgrids Driven by High Renewables. *Energies* **2019**, *12*, 3902. [CrossRef]
29. Magdy, G.; Ali, H.; Xu, D. Effective control of smart hybrid power systems: Cooperation of robust LFC and virtual inertia control system. *CSEE J. Power Energy Syst.* **2021**. [CrossRef]
30. Mishra, S.; Nayak, P.C.; Prusty, U.C.; Prusty, R.C. Frequency regulation of an islanded microgrid integrated by virtual inertia control. In Proceedings of the 2020 IEEE International Symposium on Sustainable Energy, Signal Processing and Cyber Security (iSSSC), Odisha, India, 16 December 2020; pp. 1–4.
31. Kerdphol, T.; Rahman, F.S.; Watanabe, M.; Mitani, Y.; Turschner, D.; Beck, H.-P. Enhanced Virtual Inertia Control Based on Derivative Technique to Emulate Simultaneous Inertia and Damping Properties for Microgrid Frequency Regulation. *IEEE Access* **2019**, *7*, 14422–14433. [CrossRef]
32. Abubakr, H.; Vasquez, J.C.; Mohamed, T.H.; Guerrero, J.M. The concept of direct adaptive control for improving voltage and frequency regulation loops in several power system applications. *Int. J. Electr. Power Energy Syst.* **2022**, *140*, 108068, ISSN 0142-0615. [CrossRef]
33. Long, B.; Liao, Y.; Chong, K.T.; Rodriguez, J.; Guerrero, J.M. MPC-Controlled Virtual Synchronous Generator to Enhance Frequency and Voltage Dynamic Performance in Islanded Microgrids. *IEEE Trans. Smart Grid* **2020**, *12*, 953–964. [CrossRef]
34. Magdy, G.; Ali, H.; Xu, D. A new synthetic inertia system based on electric vehicles to support the frequency stability of low-inertia modern power grids. *J. Clean. Prod.* **2021**, *297*, 126595. [CrossRef]
35. Yildirim, B.; Gheisarnejad, M.; Khooban, M.H. A New Parameter Tuning Technique for Noninteger Controllers in Low-Inertia Modern Power Grids. *IEEE J. Emerg. Sel. Top. Ind. Electron.* **2022**, *3*, 279–288. [CrossRef]
36. Fawzy, A.; Bakeer, A.; Magdy, G.; Atawi, I.E.; Roshdy, M. Adaptive Virtual Inertia-Damping System Based on Model Predictive Control for Low-Inertia Microgrids. *IEEE Access* **2021**, *9*, 109718–109731. [CrossRef]
37. Oshnoei, S.; Aghamohammadi, M.; Oshnoei, S.; Oshnoei, A.; Mohammadi-Ivatloo, B. Provision of Frequency Stability of an Islanded Microgrid Using a Novel Virtual Inertia Control and a Fractional Order Cascade Controller. *Energies* **2021**, *14*, 4152. [CrossRef]
38. Tamrakar, U.; Shrestha, D.; Maharjan, M.; Bhattarai, B.P. Virtual inertia: Current trends and future directions. *Appl. Sci.* **2017**, *7*, 654. [CrossRef]
39. Fernandez-Guillamon, A.; Gomez-Lazaro, E.; Muljadi, E.; Molina-García, A. Power systems with high renewable energy sources: A review of inertia and frequency control strategies over time. *Renew. Sustain. Energy Rev.* **2019**, *115*, 109369. [CrossRef]
40. Hashim, F.A.; Hussain, K.; Houssein, E.H.; Mabrouk, M.; Al-Atabany, W. Archimedes optimization algorithm: A new metaheuristic algorithm for solving optimization problems. *Appl. Intell.* **2021**, *51*, 1531–1551. [CrossRef]
41. Liu, L.; Liu, W.; Cartes, D.A. Particle swarm optimization-based parameter identification applied to permanent magnet synchronous motors. *Eng. Appl. Artif. Intell.* **2008**, *21*, 1092–1100. [CrossRef]
42. Kundur, P. *Power System Stability and Control*, 2nd ed.; McGraw-Hall: Ithaca, NY, USA, 1994.